

# A Low-Temperature Batch Process for the Deposition of High-Quality Conformal Alumina Thin Films for Electronic Applications

Gregory Burwell,\* Klaudia Rejnhard, Jon Evans, Jacob Mitchell, Michael T. Grimes, Matt Elwin, Ardalan Armin, and Paul Meredith\*

High-quality, alumina thin films are extensively used as dielectrics, passivation layers, and barrier layers in electronics and many other applications. However, to achieve optimum stoichiometry and thus performance, the layers are often grown at elevated temperatures ( $>200\text{ }^{\circ}\text{C}$ ) using techniques such as atomic layer deposition (ALD). This is problematic for substrates or structures with low thermal budgets. Herein, alumina thin films are grown on 200 mm silicon substrates employing a versatile deposition method known as MVD at low deposition temperatures ( $35\text{--}150\text{ }^{\circ}\text{C}$ ). The chemical composition of the resulting films is investigated postdeposition using X-ray photoelectron spectroscopy (XPS) and variable angle spectroscopic ellipsometry, with fully stoichiometric  $\text{Al}_2\text{O}_3$  achieved at deposition temperatures as low as  $100\text{ }^{\circ}\text{C}$ . Dielectric measurements confirm outstanding dielectric properties compared to typical thermal ALD layers deposited at much higher temperatures. This low-temperature deposition performance is rationalized and understood by considering the MVD reactor design and the “pump-type” regime of precursor delivery versus the “flow-type” regime of ALD is rationalized and understood. The results clearly demonstrate that alumina thin films grown with MVD are highly versatile for electronic applications and are of particular relevance and interest for the high-volume processing of dielectric, passivation, and barrier layers at low temperatures.

predominance of silicon in integrated circuits is its thermal oxide, with highly controllable properties and robustness to subsequent fabrication steps.<sup>[1]</sup> For specific applications such as surface passivation, or in next-generation materials systems such as compound semiconductors, organics and flexible electronics, thermal oxidation is either detrimental to underlying device structures or incompatible with the base materials due to high-temperature requirements and/or chemistry of the oxide process.<sup>[2,3]</sup> This has driven the development of deposition techniques for high-quality dielectric films, particularly at lower processing temperatures. In addition, the trend toward mixing different materials types *via* single system-on-chip (SoC) approaches (heterogeneous integration) raises the demand for highly conformal deposition methods that can be used to deposit within narrow, high aspect ratio features such as vias.<sup>[4]</sup>


Alumina thin films are widely reported for their suitability as high- $\kappa$  dielectrics (gates, insulators), surface passivation

layers, chemical protection barriers, etc. Atomic layer deposition (ALD) is a commonly used method to deposit high-quality, stoichiometric alumina thin films, and the reaction between trimethylaluminum (TMA) and water ( $\text{H}_2\text{O}$ ) is a standard prototypical reaction scheme to develop new ALD reactor designs.<sup>[5–9]</sup> The surface reactions of each part of the half-reactions have been

## 1. Introduction

The growth of semiconductor technologies has been in no small part due to the identification and development of stable insulating materials that allow for gate structures to be fabricated reliably and reproducibly. For example, a factor for the

G. Burwell, K. Rejnhard, A. Armin, P. Meredith  
Sustainable Advanced Materials Group  
Department of Physics, Singleton Campus  
Swansea University  
SA2 8PP Swansea, UK  
E-mail: g.burwell@swansea.ac.uk; paul.meredith@swansea.ac.uk

 The ORCID identification number(s) for the author(s) of this article can be found under <https://doi.org/10.1002/adem.202201901>.

© 2023 The Authors. Advanced Engineering Materials published by Wiley-VCH GmbH. This is an open access article under the terms of the Creative Commons Attribution License, which permits use, distribution and reproduction in any medium, provided the original work is properly cited.

DOI: 10.1002/adem.202201901

G. Burwell, K. Rejnhard, A. Armin, P. Meredith  
Centre for Integrative Semiconductor Materials (CISM)  
Bay Campus  
Swansea University  
SA1 8EN Swansea, UK

M. T. Grimes  
SPTS Division  
KLA Corp.  
Allentown, PA 18106, USA

J. Evans, J. Mitchell, M. Elwin  
Centre for Integrative Semiconductor Materials (CISM)  
Bay Campus  
Swansea University  
SA1 8EN Swansea, UK

studied in considerable detail, including the TMA<sup>[10]</sup> and the water exposure.<sup>[11]</sup> The adsorption and activation energies of these reactions have been derived from a first principles approach with good agreement to growth per cycle values (GPC—a critical figure of merit) observed experimentally.<sup>[12]</sup>

Many reports of ALD of alumina focus on deposition temperatures >200 °C, which precludes their use on substrates or devices with low thermal budgets, for example, in the field of flexible electronics. Recent reports of low-temperature ALD of alumina demonstrate the potential suitability of this material to low deposition temperatures but with variable success in delivering optimized dielectrics.<sup>[13,14]</sup> It should also be recognized that semiconductor device processing, must, like every other form of advanced manufacturing seek to minimize its embodied energy and thus carbon footprint, by, for example, reducing processing energy (temperature) inputs.

Molecular vapor deposition (MVD) is one versatile deposition technique that can allow films to be grown at low deposition temperatures (as low as 35 °C) enabling deposition onto polymer-based substrates for use in flexible electronics.<sup>[8,15,16]</sup> MVD is also a batch process widely demonstrated in the manufacturing setting with high yields and reduced embodied energies versus (for example) thermal oxides and physical vapor deposition. The MVD toolset can operate in three distinct growth modes: self-assembled monolayer, ALD, and continuous growth.<sup>[11,12]</sup> These modes can produce highly conformal films with uniform thicknesses over large wafer platforms (>200 mm). The main advantages of MVD over other thin film deposition methods include an ability to deposit at low growth temperatures, deposition of conformal films on high aspect ratio features (5000:1), and a large sample chamber, for high throughput processing. MVD tools can deposit several film types, using a combination of the deposition modes if required, on the same substrate in a multicycle or supercycle mode.<sup>[17,18]</sup>

MVD differs from related methods such as chemical vapor deposition (CVD) and conventional ALD since the MVD process does not require a continuous flow of precursor materials.<sup>[19–21]</sup> Many ALD systems utilize a “continuous flow” type reaction. In this instance, an uninterrupted flow of nitrogen gas passes through the reaction chamber and acts as the chamber purge, but also as the carrier gas for the precursor during the deposition cycle. The precursor molecules must diffuse through the carrier gas to reach the active sites present on the substrate to initiate film growth.

In MVD, there are repeated and sequential exposures of the substrate to precisely delivered precursors. As such, multiple atomic layers are deposited to create single-component, multi-layer, or composite thin films with engineered properties for applications, such as semiconductors devices, antistiction layers, photovoltaics, and metal–organic frameworks.<sup>[22–24]</sup>

In this study, an MVD batch-process method was developed for the deposition of alumina at low growth temperatures (35–150 °C). Thin alumina films were grown on 8” silicon substrates using thermally reacted precursors of trimethylaluminum (TMA) and deionized water (DI H<sub>2</sub>O), under an ALD-type reaction in the “pump-type” regime. The chemical composition and optical properties of the deposited films [including stoichiometry and refractive indices (RI)] were investigated using a combination of techniques. Impedance measurements were

performed on films deposited on silicon substrates to measure the dielectric constants for direct structure-property comparison. In addition, exemplary capacitor structures were fabricated on ITO/PET films grown at 100 °C, demonstrating the suitability of our MVD alumina process with low thermal budgets. To elucidate the process differences between the MVD growth regime and alternative ALD-type reactors, the precursor delivery kinetics were analyzed with a hypothesis advanced as to why the MVD process produces such high-quality films at low deposition temperatures.

## 2. Results

### 2.1. Process Evolution

A full series of carefully designed process optimization experiments were conducted to develop the MVD deposition method for alumina on Si substrates. These were separated into two main studies: the dosing of the precursors and the reaction temperature (between 35 and 150 °C). These variables establish the process linearity and uniformity windows. Spectroscopic ellipsometry was used to measure the film RI and the thicknesses profile over a full wafer, thus allowing for the baselining of material quality, uniformity, and GPC. In addition, X-Ray photoelectron spectroscopy (XPS) was used to assess the stoichiometric outcomes in the reaction temperature study.

It is worth noting that so-called “vapor delivery modules” (VDMs) are employed in MVD to accurately control the precursor dosing levels to the desired pressures, which equate to a known volume (approximated by the ideal gas law). When triggered, the VDM discharges the pressurized vapor, which is drawn into the heated reaction chamber *via* a nozzle driven by the relative pressure differential. A schematic of the precursor delivery mechanism is provided by way of illustration in Figure S1, Supporting Information.

### 2.2. Precursor Dosing

A study was performed to determine the precursor saturation point for both TMA and water, under constant chamber temperature (100 °C) with a fixed number of deposition cycles, set at 576 to achieve a minimum thickness of 50 nm. The precursor saturation points were independently assessed by fixing one precursor pressure level and varying the second between a minimum and maximum pressure (0.4–4 Torr for TMA and 0.4–5 Torr for water). Subsequent analysis of the resultant films for properties (RI, GPC, nonuniformity) revealed the precursor saturation points for TMA and water to be 1.3 and 1 Torr, respectively. The results are shown in **Figure 1a,b**.

During the precursor dosing study, it was noted that an increase in water vapor within the chamber, results in significantly higher GPC when compared to increasing TMA dosing pressure (which results in a flat response when overdosing). GPC results are also reflected in RI trends for both precursors. There are several factors contributing to the final decision of precursor dosing. The priority was the main aspect of assessing the saturation point in which all active sites are utilized, beyond which there is no or very little growth. Increasing water vapor

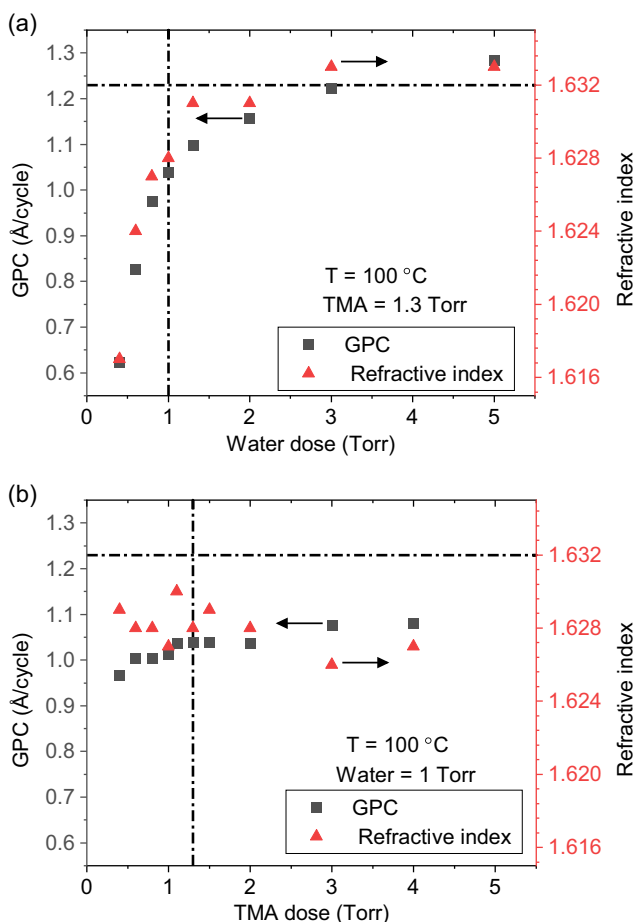


**Figure 1.** Precursor dosing study for the MVD alumina growth per cycle (GPC) and refractive index (RI) measured as a function of a) water dose and b) TMA dose. The data indicate that the precursor saturation partial pressures were, respectively, 1.0 and 1.3 Torr for water and TMA.

dosing beyond 1 Torr affected the RI of deposited films, suggesting that the alumina composition was oxygen-rich ( $RI > 1.63$ ). Overdosing water vapor carries additional complications when purging unreacted water preventing it from reacting with TMA, which can lead to CVD deposition of alumina on top of the ALD-deposited film. When dosing TMA at values higher than 1.3 Torr, there was no significant increase in GPC observed. Hence, we arrived at the 1.0 Torr:1.3 Torr combination.

### 2.3. Reaction Temperature

The reaction temperature study was designed to investigate the film properties at deposition ranging between 35 and 150 °C. At each temperature, the number of cycles (576) and precursor dosing pressures (1 Torr water, 1.3 Torr TMA) were kept constant. The results from these depositions and related optical measurements are shown in **Figure 2a**, which presents GPC and RI as a function of reaction temperature.

We found the following: at temperatures above 60 °C, the GPC (**Figure 2a**) increases until it reaches 120 °C, and RI (**Figure 2a**) also steadily increases until 150 °C. Films deposited at 35 °C

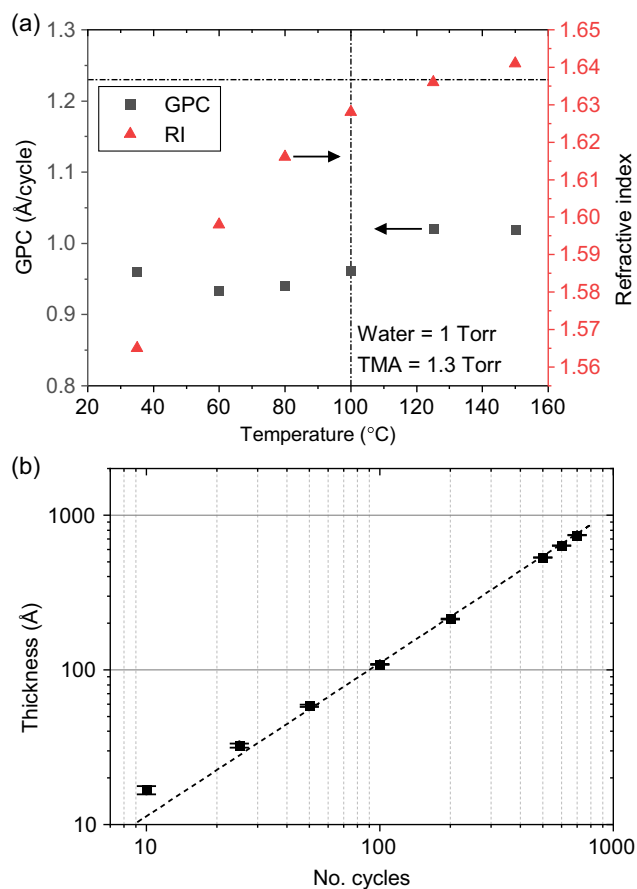


**Figure 2.** a) Deposition temperature study for MVD alumina—maximum theoretical GPC for a self-limiting process indicated by the horizontal line, with the vertical line indicating the default deposition temperature for the dosing study. b) The thickness of the deposited films as a function of the number of cycles (points). The dashed line corresponds to a unity logarithmic slope. Process conditions 100 °C, 1.0 Torr TMA, and water to reduce material consumption during longer processes.

display a high GPC, but they are not comparable in terms of stoichiometry and RI to those grown at higher temperatures. Their low refractive index ( $\approx 1.56$ ) and stoichiometry (see stoichiometry by XPS section) indicate that films grown at 35 °C have low densities and contain significant organic impurities which originate from unreacted TMA precursor (e.g., methyl groups).<sup>[21]</sup> Optimal RI indicative of stoichiometric materials and dense films are obtained at reaction temperatures  $>100$  °C, and above this region, one also observes a plateauing of the GPC.

### 2.4. Process Linearity

Linearity is a key control parameter for any reproducible deposition process and is a measure of the stability of GPC across the required range of deposition cycles (and thus film thickness).<sup>[24,25]</sup> In this regard, for the MVD alumina process linearity validation, the precursor doses were kept constant at 1 Torr for both TMA and water, whilst the deposition temperature was fixed at 100 °C and the number of deposited cycles varied from 10 up to

a maximum of 700. As shown in Figure 2b, the resultant film thickness was observed to be linear across the evaluated range, at the selected process conditions. An apparent slight sublinearity is observed at small cycle numbers that are related to the uncertainty of the thickness measurements for very thin samples (<30 Å). This is consistent with other reports, including Vandalon et al., which report varying GPC on the initial few cycles, depending on Si surface termination.<sup>[25]</sup> The overall linearity of the process indicates that the deposition of alumina by MVD in the chosen process window does not follow an accelerated or delayed growth regime. We note that the TMA dosing rate of 1.0 Torr was chosen to minimize material consumption whilst being within the dosing saturation regime, as shown in Figure 1b.

## 2.5. Uniformity and Batch Processing

The suitability of MVD for full-wafer and multiwafer batch processing was also studied. First, the effect of the process parameters was investigated as a function of intrawafer uniformity—these studies being extensions of dosing and reaction temperature by mapping the full wafer thickness and thus determining a nonuniformity (NU), defined as

$$NU = \frac{(MAX - MIN)}{(2 \times MEAN)} \times 100\% \quad (1)$$

where MAX, MIN, and MEAN are the maximum, minimum, and mean thicknesses, respectively.

The effects of precursor dosing on deposition nonuniformity are shown in Figure 3a where there is a clear optimum regime of between 1 and 2 Torr for both precursors. This can be understood in terms of the spatial availability of precursor with respect to consumption and will be discussed later in the manuscript. A similar trend is seen as a function of deposition temperature, shown in Figure 3b, where there is maximum uniformity achieved between 80 and  $\approx 120$  °C although we stress that a NU of <1.3% is still exceptionally low over an 8" wafer and thus 150 °C would be a perfectly acceptable process temperature.

The effect of chamber loading (number of wafers in a stacked batch) was studied to understand how these parameters are related to interwafer uniformity for batch processing. In this study, the effective surface area was increased by running 5 and 25 wafers per batch. Runs with 1, 5, and 25 wafers (the maximum for our chamber design) were undertaken to establish the effect of higher area load on the GPC and nonuniformity of the deposited thin films. The number of cycles was fixed at 576 in this study, with the same wafer carrier present in the chamber for all depositions for consistency. The wafers were fixed in the following holder positions, 1, 5, 10, 20, and 25, again for consistency and to minimize experimental variables. The process parameters were 1.0 Torr water, 1.3 Torr TMA, and 100 °C.

With a single 8 inch wafer loaded in the chamber, 602 Å was deposited (GPC = 1.04), with excellent intrawafer NU as indicated above. The experiment was repeated with 5 and 25 wafers present in the chamber. A five-wafer run gave an average thickness of 582 Å, with the variation in thickness between the five wafers being 8.8 Å, corresponding to an average nonuniformity of 0.76 %, with the GPC varying from 1 to 1.02 Å/cycle, i.e.,

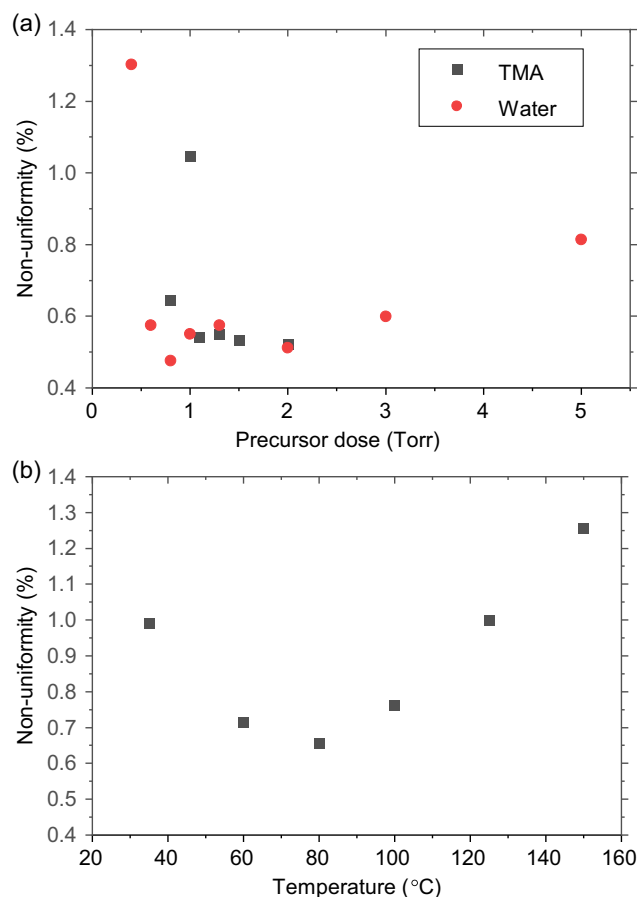


**Figure 3.** Intrawafer nonuniformity (NU) as a function of a) precursor dose and b) deposition temperature.

slightly reduced versus the single wafer but still demonstrating excellent process control.

Increasing the number of wafers to 25 within the reaction chamber also demonstrated highly stable and uniform batch processing capability, with only small changes to GPC ( $\approx 0.8$  Å cycle<sup>-1</sup>) across the sampled wafers as one might expect with the substantially increased deposition surface area. The nonuniformity was also found to be comparable between the 5- and 25-wafer loading studies. The average nonuniformity for the 25-wafer study was 0.81% and the average thickness of 477.62 Å.

Figure 4a summarizes these data for loadings of 1, 5, and 25 wafers with GPC and NU also shown as a function of the wafer slot (position in the chamber). Here, the blue line represents a benchmark GPC of 1.04 Å/cycle, which is an indicative growth rate when only one wafer is loaded in the chamber. The reduction in GPC for both the 5- and 25-wafer studies can be attributed to the increased number of active sites present, meaning higher precursor dosing is required to achieve recovery of the GPC to the value observed with a single loaded wafer (1.04 Å cycle<sup>-1</sup>). The RI of the deposited films were also found to be consistent and are likewise summarized in Figure 4b.

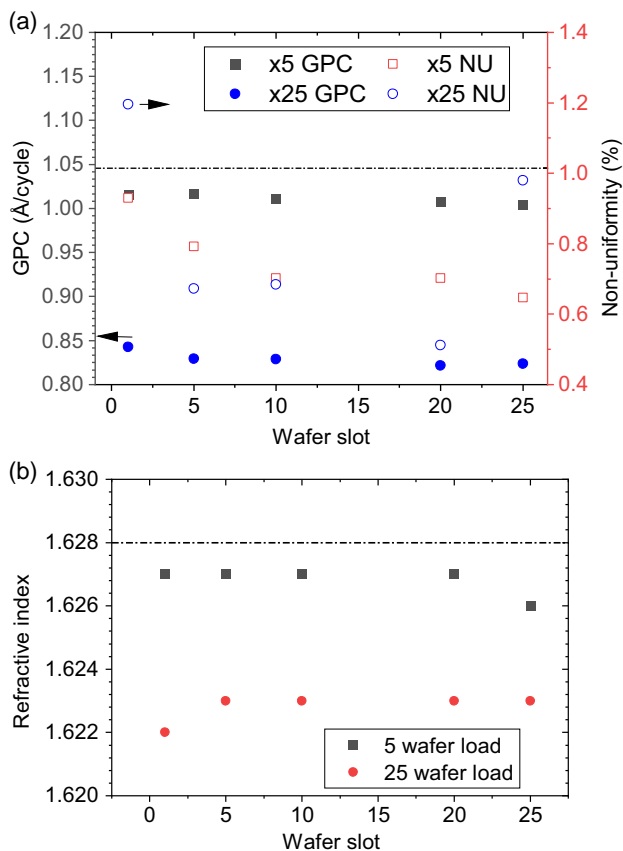


**Figure 4.** The effect of chamber loading (i.e., the interwafer batch variability) on a) GPC and NU and b) refractive index. The single-wafer deposition values are shown as horizontal lines.

## 2.6. Stoichiometric Evaluation via X-Ray Photoelectron Spectroscopy (XPS)

The stoichiometries of MVD alumina thin films were measured using XPS with a particular focus on the deposition temperature which is expected to be a first-order control variable for composition.<sup>[26]</sup> A commercially grown single crystal alumina (sapphire) sample was run alongside the MVD deposited films as a reference and internal calibration. Survey spectra were collected before and postetch with an Ar<sup>+</sup> cluster gun to remove adventitious carbon on the surfaces of the deposited films. XPS was chosen as the primary chemical analytical tool since its sampling depth is suited to our studied film thicknesses ( $\approx 50$  nm), and it is particularly good at identifying and, through careful calibration and peak fitting, quantifying the relative atomic compositions to deliver the accurate stoichiometric value of O: Al.

The results of the O: Al ratio derived from Survey Scans (an example being Figure 5c) are shown in Figure 5a for deposition temperatures between 30 and 150 °C. The stoichiometric values were derived from the O1s peak at 529.40 eV, C1s at 283.00 eV, Al 2p at 73.00 eV, and Al 2s at 117.80 eV (Al 2p was used for O: Al calculations).<sup>[22,23]</sup> The ratio decreases with increasing deposition temperature, which suggests that deposited films are relatively

oxygen-rich at low temperatures, consistent with the trends seen in previous works.<sup>[26]</sup> We find that fully stoichiometric (O: Al = 1.5) alumina was deposited at 100 °C. This is also consistent with RI measured in the dosing and reaction temperature study (dense stoichiometric alumina having an archetypal refractive index of 1.628).

High-resolution spectra of the C1s peak were collected and analyzed showing that the carbon content of the films decreases with increasing deposition temperature (Figure 5b). The sapphire crystal was also used to calibrate the Ar<sup>+</sup> etch, such that all adventitious carbon was removed without affecting the bulk of the deposited film. The presence of sp<sup>3</sup>-bonded carbon is the main source of contamination for the deposited alumina films. The spectra of C1s were studied in detail to eliminate confusion between carbon which is present as contamination on the surface of the sample and carbon present in the bulk of the film (indicated by different binding energy). The C1s peak was significantly reduced by the in situ surface etching, reaching the noise level of the measurement at deposition temperature >60 °C, as determined by the sapphire crystal. Components of C1s were analyzed and the main contribution was from C–C, and C–H at 284.93 eV, the additional peaks were identified as C–O at 286.85 and C=O at 289.82. These very clear XPS measurements confirm the observations from the optical studies and should thus also be reflected in the dielectric analysis.

## 2.7. Dielectric Measurements

The dielectric properties of the MVD alumina thin films were measured using a mercury probe system (described in Figure S2, Supporting Information) in a metal–insulator–semiconductor configuration and the results are presented in Figure 6. Figure 6a shows examples of the first (solid line) and third (dashed line) capacitance–voltage (C–V) curves obtained at each deposition temperature. Hysteresis is evident between sweep directions, with anticlockwise hysteresis observed for all deposition temperatures except for 35 °C, which exhibits clockwise hysteresis typically associated with mobile charge effects<sup>[27,28]</sup> indicating a transition in film composition between the 35 and 60 °C. The remainder of this discussion will focus on the deposition temperatures of 60 °C and above as representative dielectric systems. The flat band voltage ( $V_{fb}$ ) for both sweep directions was determined from the flat band capacitance ( $C_{fb}$ ), calculated using the following equation

$$C_{fb} = \frac{C_{ox}\epsilon_{Si}A/\lambda_D}{C_{ox} + \epsilon_{Si}A/\lambda_D} \quad (2)$$

where  $C_{ox}$  is the accumulation capacitance,  $\epsilon_{Si}$  is the relative permittivity of silicon (11.68),  $A$  is the calibrated mercury probe area, and  $\lambda_D$  is the Debye length

$$\lambda_D = \sqrt{\frac{\epsilon_{Si}k_B T}{q^2 N_a}} \quad (3)$$

The substrate doping concentration, ( $N_a$  10<sup>16</sup> cm<sup>-3</sup>), was extracted from the C–V curves using the Mott–Schottky method and the parameters outlined above<sup>[27]</sup> In the absence of fixed

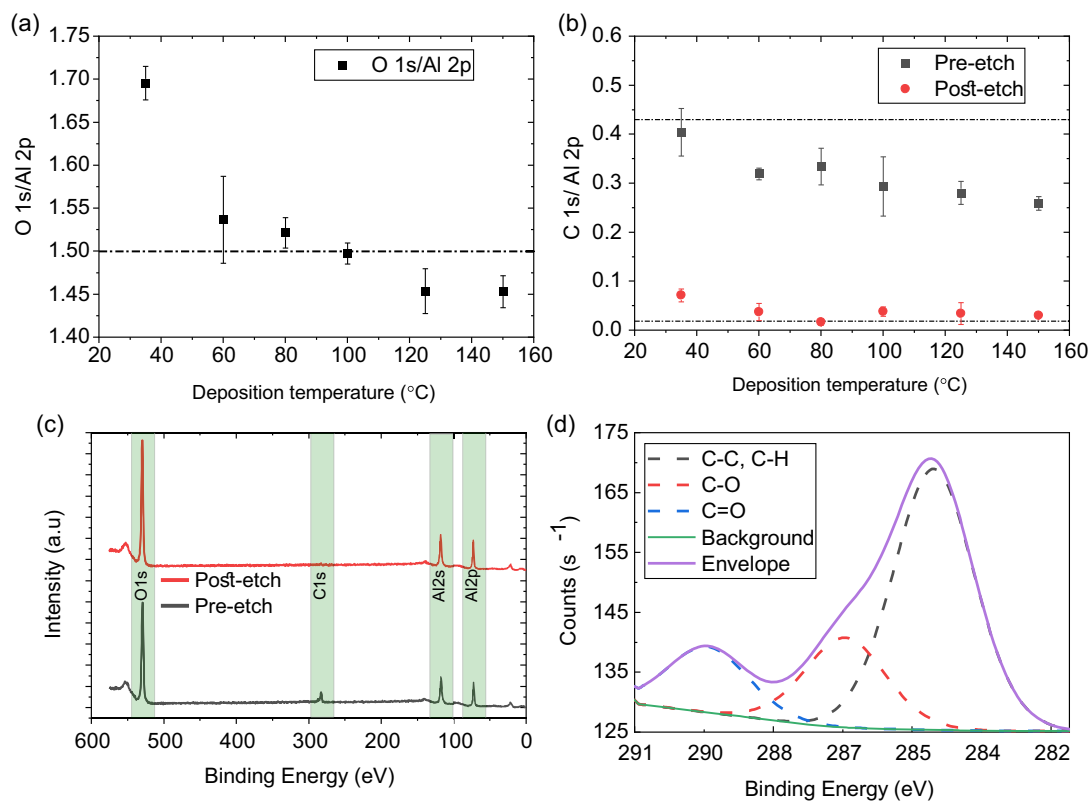


**Figure 5.** Effect of deposition temperature on the stoichiometry of MVD alumina films measured using X-ray Photoelectron Spectroscopy (XPS). a) The ratio of the measured O: Al (measured using O 1s and Al 2p core levels). The dashed line signifies the O 1s: Al 2p ratio in a single crystal (run alongside the process samples as a calibration). b) Carbon content in the films (before and after 100 s etch with an Ar<sup>+</sup> cluster source 5 keV for 100 s) displayed as C 1s: Al 2p ratio with varying deposition temperatures. The dashed line signifies the changing carbon content in the single crystal (run alongside the process samples). Survey spectra of MVD deposited alumina films (100 °C) showing O 1s, C 1s, Al 2s, and Al 2p core levels. c) High-resolution spectra showing fitted components of C 1s d) before etching took place with the Ar<sup>+</sup> cluster source—5 keV for 100 s.

charges, the flat band voltage is equal to the work-function difference between the metal electrode and the *p*-type silicon semiconductor

$$qV_{fb} = \Phi_{MS} = \Phi_M - \chi - \frac{E_g}{2} - k_B T \ln\left(\frac{N_a}{N_i}\right) \quad (4)$$

where  $\Phi_M$  is the mercury work function (4.53 eV) and  $\chi$ ,  $E_g$  and  $N_i$  are the silicon substrate electron affinity (4.05 eV), bandgap (1.12 eV) and intrinsic carrier concentration ( $10^{10} \text{ cm}^{-3}$ ), respectively. These values result in a calculated flat band voltage of  $-0.44 \text{ V}$ . For deposition temperatures of  $100 \text{ }^\circ\text{C}$  and below, the flat band voltage extracted from the negative to positive sweep direction is less than  $-2 \text{ V}$ , as indicated by the dashed vertical lines in Figure 6a. This indicates the presence of fixed positive charges (ions) in the oxide, which appear to decrease with increasing deposition temperature (increase in  $V_{fb}$ ). For the  $125 \text{ }^\circ\text{C}$  deposition, the flat band voltage extracted from this half cycle is  $-0.96 \text{ V}$ , approaching the calculated value of  $-0.44 \text{ V}$ . With the  $150 \text{ }^\circ\text{C}$  deposition,  $V_{fb}$  increases above the calculated value to  $-0.02 \text{ V}$ . Typically, ALD-alumina layers deposited at  $>150 \text{ }^\circ\text{C}$  are associated with the presence of fixed negative charges,<sup>[29,30]</sup> as observed for the  $150 \text{ }^\circ\text{C}$  deposition with

$qV_{fb} > \Phi_{MS}$ . The positive-to-negative sweep results in  $V_{fb} > 0 \text{ V}$ , which is unstable under repeated voltage cycling (shaded area of Figure 6a). Anticlockwise hysteresis with a shift to higher  $V_{fb}$  is suggestive of slow near-interface acceptor states (e.g., border traps<sup>[31,32]</sup>), which are filled during the deep depletion part of the cycle, resulting in a shift in the C–V curve to positive gate voltages (described in Figure S2, Supporting Information). Previously, the physical origin of built-in negative charge has been attributed to acceptor-like traps,<sup>[32]</sup> which have been associated with oxygen-rich conditions in films.<sup>[33,34]</sup> It should be noted that the gradient of the depletion part of the C–V curves is relatively constant across deposition temperatures, indicating a similar value for the density of “fast” interface traps ( $D$ ) that can directly exchange charge carriers with silicon. This could be explained by the thin native  $\text{SiO}_x$  layer governing the near-interface trap states.<sup>[30,34]</sup> The incomplete adsorption of TMA molecules during the initial growth cycles has been used to explain high negative charge density near the interface.<sup>[33]</sup> For lower deposition temperatures, where the incomplete reaction of TMA molecules may be expected in the bulk of the films, a higher density of positive fixed charge is observed (negative shift in  $V_{fb}$ ), but also correlated with an increase in electron traps (increased hysteresis).

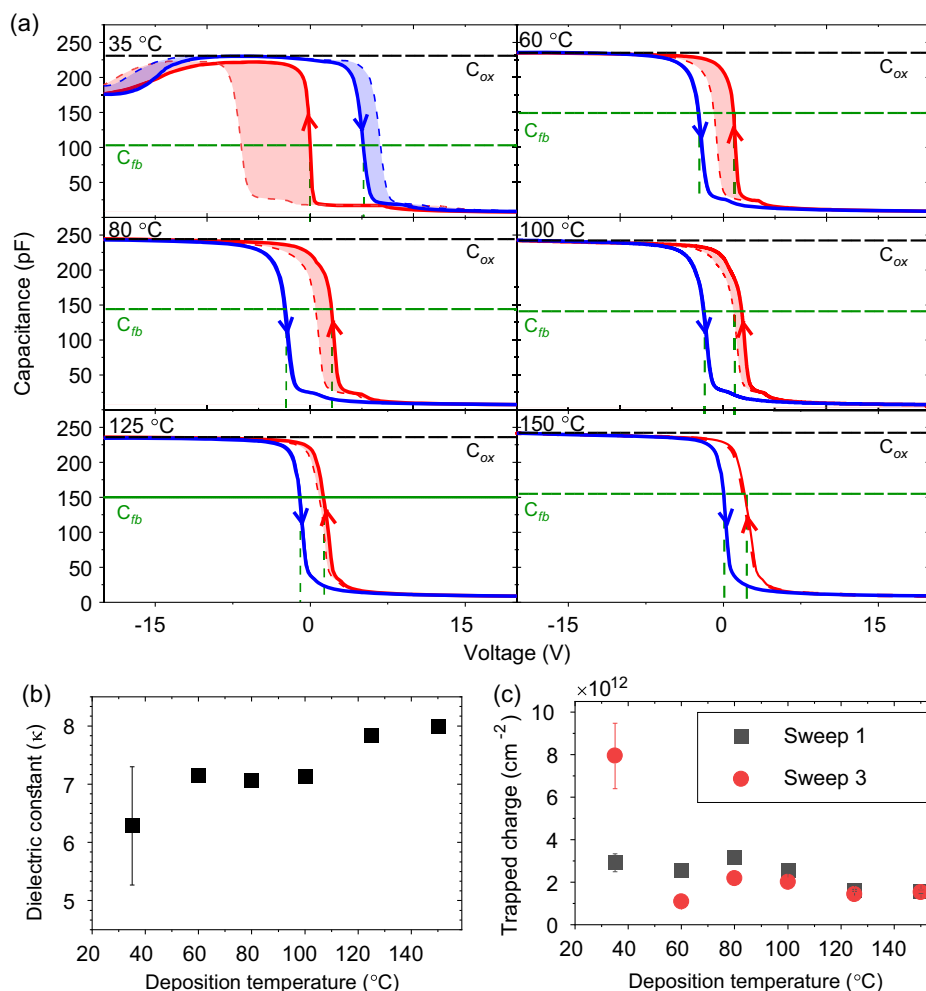


**Figure 6.** a) Capacitance–voltage ( $C$ – $V$ ) curves for MVD alumina films deposited at different temperatures, measured at a frequency of 1 MHz. Voltage cycles were started in depletion (20 V), swept to accumulation (red line,  $-20$  V), before returning to depletion (blue line). The dashed  $C$ – $V$  curves show the behavior after three complete cycles, with the filled areas highlighting the shift in flat band voltage. b) Equivalent dielectric constant extracted from  $C_{ox}$  using a basic parallel plate model. c) The magnitude of total trapped charge extracted from  $\Delta V_{fb}$  of  $C$ – $V$  curves after one sweep and three sweeps, demonstrating the effect of initial bias stress on oxide traps.

The difference in flat band voltage between sweep directions,  $\Delta V_{fb}$ , can be used to estimate the total trapped charge in the films by multiplying by the oxide capacitance, as shown in previous reports.<sup>[35,36]</sup> Figure 6c shows the absolute trapped charge density as a function of deposition temperature. In addition to the general trend of reduced trapped charge with increasing temperature, for the films deposited in the range 60–150 °C, there is a reduction in trapped charge following voltage cycling between sweeps 1 and 3. This is a consequence of the change in  $V_{fb}$  in the depletion to accumulation sweep direction, indicated by the filled areas in Figure 6a, and is consistent with a reduction of near-interfacial oxide acceptor traps following negative bias stress under strong accumulation. The degree to which these traps are reduced under negative bias, and consequently the stability of the dielectric under initial bias stress, also appears to be dependent on deposition temperature, with little change seen between sweeps 1 and 3 for the 150 °C deposition ( $1.49 \times 10^{12}$  to  $1.41 \times 10^{12} \text{ cm}^{-2}$ ). In general, the density of trapped electrons

is typical of previous studies of the Si–SiO<sub>x</sub>–alumina interface,<sup>[30,33,34]</sup> despite the lower temperature for the MVD process compared with conventional ALD.

As mentioned above, the film deposited at 35 °C showed different behavior under repeated cycles, with  $V_{fb}$  instability in both sweep directions and  $\Delta V_{fb}$  continuing to increase. It should be noted that measurements on initial bias stress are not intended to be extrapolated to long-term reliability but indicate that initial chemical/structural changes in the films are expected at lower deposition temperatures under relatively high electric fields ( $\approx 4 \text{ MV cm}^{-1}$ ).

The equivalent dielectric constant of the MVD alumina films was determined from the accumulation region of the  $C$ – $V$  curve using the mercury probe capacitor area and oxide thicknesses obtained using ellipsometry, assuming a basic parallel plane capacitor model. The dielectric constant (Figure 6b) increases at higher deposition temperatures, approaching the typical value of  $\kappa \approx 8$  for ALD alumina at 100–130 °C.<sup>[37]</sup> For the 35 °C

deposition temperature, a lower dielectric constant was generally measured, with considerable variation in maximum accumulation capacitance between measurement locations. This lower  $C_{ox}$  can be attributed to low resistance in parallel with the oxide capacitance, suggesting a high leakage current in agreement with the decrease in capacitance observed under strong accumulation.

Leakage and breakdown measurements were conducted using the mercury probe in a vertical (through-wafer) configuration. Figure S3, Supporting Information, shows low leakage currents (noise level) for electrical fields  $<6 \text{ MV cm}^{-1}$ , with the exception of the  $35^\circ\text{C}$  deposition, which formed a high resistance rectifying contact. A slightly higher leakage characteristic is seen for the  $60^\circ\text{C}$  deposition before breakdown; however, a similar breakdown of  $\approx 9 \text{ MV cm}^{-1}$  was measured across the films, with no improvement seen for the  $125$  and  $150^\circ\text{C}$  deposition temperatures indicating the attainment of a dielectric optimum.

To demonstrate the applicability of this process to substrates with low thermal budgets, thick alumina films were deposited onto indium tin oxide/polyethylene terephthalate (ITO/PET). Dielectric measurements of these metal–insulator–metal type structures were conducted similarly to those described on Si. Figure S4, Supporting Information, shows that the dielectric constant of the deposited films was similar to that achieved on silicon.

In summary, these dielectric measurements confirm the optical and chemical analyses indicating that deposition temperature  $>100^\circ\text{C}$  or so deliver high quality, dense, stoichiometric dielectric thin films of alumina with high reproducibility and low nonuniformity over an  $8''$  silicon wafer.

### 3. Discussion

As the TMA/water system is a well-known archetypical reaction used for deposition reactor development, the values obtained in this work serve as a useful comparator between reactor designs. The MVD system used here is a *pump-type* reactor, in which the precursor gases are injected into the chamber without the use of a carrier gas. This type of reactor design is distinct from typical ALD reports, which focus on the development and optimization of flow-type systems. These reactors use a flow of inert carrier gas to assist the delivery of precursor into the reaction chamber and typically use much shorter cycle times (10 s). Flow-type reactors are predominantly reported for this reason, and high-quality alumina films have been demonstrated using this technique, particularly at higher deposition temperatures ( $>250^\circ\text{C}$ ).

To understand why the MVD-type reactor design produces alumina films with close to ideal stoichiometry at low deposition temperatures, it is informative to compare the physical processes involved in precursor delivery in the two systems. In general, the mean free path  $\lambda$  of a molecule of a particle (species A) in a carrier gas (species B) is given by

$$\lambda_{0,A} = \frac{k_B T}{(\sqrt{2}P_A\sigma_{A,A}) + \left(\sqrt{1 + \frac{m_A}{m_B}P_B}\sigma_{A,B}\right)} \quad (5)$$

with  $T$  being the temperature (K),  $P_i$  the partial pressure, and  $m_i$  the molecular masses, and  $\sigma_{A,B}$  the scattering cross-section is given by

$$\sigma_{i,j} = \pi(r_i + r_j)^2 \quad (6)$$

where  $r_i$  is the effective molecular interaction radius of species  $i$ . In the absence of a carrier gas, this expression simplifies to

$$\lambda = \frac{k_B T}{\sqrt{2}P_A\sigma_{A,A}} \quad (7)$$

At a given temperature and pressure,  $\lambda$  will be greater in a carrier-gas-free system, as only self-scattering is possible. Estimates for the mean free path in a pump-type and flow-type reactor are shown in Figure 7a,b. The difference in the mean free path affects the type of flow attainable to penetrate narrow structures. This can be quantified by the dimensionless Knudsen parameter  $Kn$  is given by

$$Kn = \frac{\lambda}{d_p} \quad (8)$$

where  $d_p$  is the pore diameter of the feature being considered. In the case  $Kn \gg 1$ , gas transport is said to be in the molecular-flow regime, where particle-surface interactions dominate. When  $Kn \ll 1$ , flow is said to be in the viscous regime, where particle–particle interactions dominate.

In the MVD system, the fill pressures of the VDM of each precursor are critical, influencing both the dose of precursor injected in each half-cycle and the uniformity of the deposited film. The delivery of precursors from the VDM into the reaction chamber can be approximated using the Bernoulli equation for an incompressible fluid of uniform density<sup>[38]</sup>

$$P_1 + \frac{1}{2}\rho v_1^2 + \rho g h_1 = P_2 + \frac{1}{2}\rho v_2^2 + \rho g h_2 \quad (9)$$

where  $\rho$  is the density of the precursor gas,  $P_1, v_1, h_1$  are the pressure, velocity, and height of the precursor in the VDM, and  $P_2, v_2, h_2$  are the variables inside the reaction chamber. Rearranging for the case  $h_1 = h_2, v_1 = 0$  gives

$$v_2 = \frac{\sqrt{2(P_1 - P_2)}}{\rho} \quad (10)$$

i.e., the velocity of the injected precursor depends primarily on the difference in pressure between the VDM and reaction chamber, in line with basic intuition. This behavior is evidenced in Figure 3a, in which the nonuniformity of alumina deposition increases at very low precursor doses for both TMA and water ( $<1$  Torr). This suggests that the pump reactor layout has a much more stable operational parameter space than its flow-reactor counterparts. Similarly, the mean free path of the injected precursor being larger will impact film uniformity, particularly within pores or tortuous features.

During each half-cycle, the precursor gas is introduced into the reaction chamber with the mean velocity given by (10). The effective diffusion coefficient in a pump-type reactor is given by the product of the mean velocity and the mean free path

$$D_{\text{pump}} = \lambda \times v \quad (11)$$

which is the product of expressions (7) and (10)



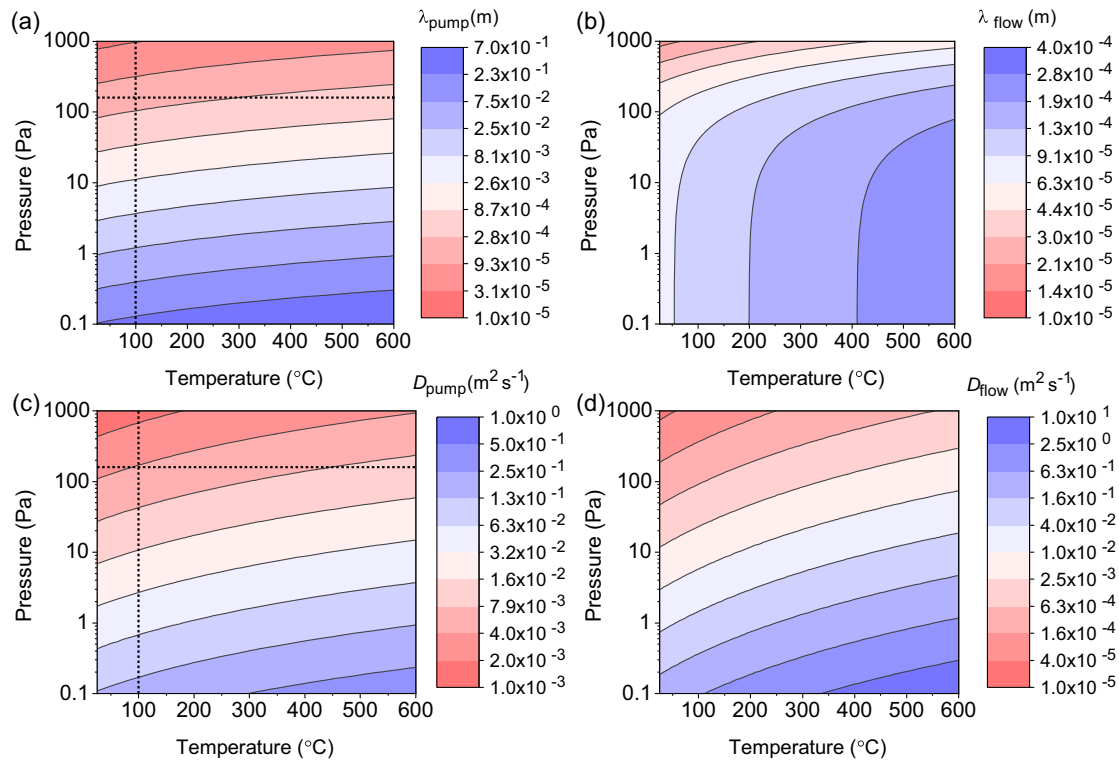


**Figure 7.** Comparison of the water half-cycles in pump-type (such as MVD) and flow-type reactors a) mean free path for a pump-type system. b) Mean free path in flow-type reactors. c) Diffusion coefficients in a pump-type reactor, d) diffusion coefficients in a flow-type reactor. Typical process temperatures and pressures are given by the vertical and horizontal dashed lines, respectively.

$$D_{\text{pump}} = \frac{k_B T}{\sqrt{2} P_A \sigma_{A,A}} \cdot \frac{\sqrt{2(P_1 - P_2)}}{\rho} \quad (12)$$

In contrast, ALD reactor designs that utilize a flow of carrier gas to deliver precursors to the reaction chamber deliver a mixture of the precursor and the carrier gas to the reaction chamber. The diffusion constant of gas A in gas B is given by the Chapman–Enskog formula<sup>[39]</sup> and can be used to estimate the diffusion of the precursor in a carrier gas in a flow-type system

$$D_{\text{flow}} = \frac{\sqrt{\left\{ \frac{9(RT)^3}{8\pi} \left( \frac{1}{m_A} + \frac{1}{m_B} \right) \right\}}}{(\sigma_A + \sigma_B)^2 P_{\text{tot}} \Omega N_A} \quad (13)$$

where  $P_{\text{tot}}$  is the total pressure,  $m_i$  the molecular mass,  $\sigma_i$  the scattering cross-section of the molecule,  $\Omega$  the diffusion collision integral, and  $N_A$  Avogadro's constant. The collision integral  $\Omega$  can be approximated by  $\Omega = \left(\frac{370}{T}\right)^{0.25}$  in nitrogen. This approximation gives  $D_{\text{flow}} \propto T^{1.75}$  dependence, whereas  $D_{\text{pump}}$  is assumed to be linear with temperature in this model. Estimates for the effective diffusion coefficients are shown in Figure 7c,d for a pump and flow-type reactor, respectively.

The exact diffusion coefficients for a particular reactor system will depend on several factors, not limited to the partial pressures, reactor geometry, and gas temperature. However, this difference in temperature dependence will be present in any system utilizing a carrier gas to introduce precursor to the chamber,

indicating that a flow-type system capable of producing high-quality films in a higher temperature regime may have very different reaction kinetics when the temperature is reduced.<sup>[30,31,35,36]</sup> In summary, this simple model shows that pump-type reactor designs have inherent advantages in terms of reaction kinetics at low deposition temperatures, which in turn influence deposition uniformity and conformality.

### 3.1. Comparative Analysis

In drawing together this discussion, it is valuable to perform a comparative analysis between these MVD alumina films and those reported using related techniques. First, in this and previous works, alumina films deposited at low temperatures appear oxygen-rich, suggesting the hydroxide groups are prominent, which are not fully utilized by the reaction with TMA.<sup>[26]</sup> Although this can be improved by using alternative O sources compared to a thermal H<sub>2</sub>O reaction (such as O<sub>3</sub> plasmas) to lower the activation energy. XPS and dielectric data show clear agreement with this hypothesis. Stoichiometric alumina was deposited by MVD at temperatures as low as 80 °C. The O: Al ratios of films deposited at 80 and 100 °C were 1.52 and 1.50, respectively.

The use of thermal TMA/H<sub>2</sub>O processes to deposit alumina has been widely reported in previous works and has been covered in multiple reviews.<sup>[20,40–45]</sup> The deposition temperatures for the MVD process for alumina reported are typically lower than that

of ALD films detailed in the literature, particularly those considered for dielectric applications.<sup>[45]</sup> Lower temperature ALD alumina depositions have been reported, particularly in situations where the dielectric properties are less critical, including passivation and barrier film applications. Low-temperature ALD deposition has been reported (down to 33 °C), with effective barrier films deposited onto PET at 58 °C in a flow-type system.<sup>[18]</sup> Thin alumina films have been used in organic light-emitting diodes (OLEDs) deposited at 80 °C using optimized process parameters.<sup>[46]</sup> The thermal conductivity of the barrier films used in OLED applications is an important consideration due to the thermal degradation of the light-emitting material.<sup>[47]</sup>

The electrical characteristics of the films reported in this work follow similar trends to low-temperature alumina films deposited for dielectric applications in the literature. The dielectric constants reported across the deposition temperature range in this work ( $\kappa \approx 7\text{--}8$ ) are consistent with previous reports of <150 °C deposition in the literature.<sup>[18,42,45,48]</sup> Interestingly, the breakdown field reported here ( $\approx 9 \text{ MV cm}^{-1}$ ) is significantly higher than comparable reports from a flow-type reactor system ( $4.4 \text{ MV cm}^{-1}$  from a 177 °C deposited film<sup>[18]</sup>), and similar to early reports using a pump-type reactor ( $\approx 8 \text{ MV cm}^{-1}$  from a 177 °C deposited film<sup>[48]</sup>). This may indicate that pump-type reactions are less prone to breakdown-inducing impurity inclusions at comparable deposition temperatures.

It is informative to compare the stoichiometry of alumina films deposited at various temperatures. Naumann et al. reported a deposition temperature for alumina using ALD of 220 °C, followed by postdeposition annealing at 500 °C, to achieve a stoichiometry of 1.65.<sup>[49]</sup> Barbos et al. deposited thin films of alumina samples between 2 and 100 nm thick using ALD. Samples were observed to have a RI of 1.65 and a GPC of  $0.98 \text{ \AA cycle}^{-1}$ . Depositions took place at 250 °C, with further postdeposition annealing required at 400 °C to provide a stoichiometry by XPS of 1.87 for a 4.7 nm and 1.7 for a 14.7 nm sample.<sup>[50]</sup> Gakis et al. deposited alumina at 300 °C, whereby the stoichiometry was close to 1.5 and a GPC of  $1 \text{ \AA cycle}^{-1}$ . ALD deposited alumina at 250 °C and annealed at 400 °C produced film stoichiometries of 1.55.<sup>[51]</sup> Hemmen et al. deposited alumina at a range of temperatures (25 up to 300 °C) using thermal and Plasma Enhanced-ALD achieving a stoichiometry of 1.7 at 35 °C and 1.5 for films deposited at 200 and 300 °C. For deposition temperatures below 300 °C, the dielectric constants reported were 7.6 or lower.<sup>[52]</sup> Zakirov et al. also reported ALD-deposited alumina with an O: Al ratio of 1.4.

Stoichiometric ratios lower than 1.5 suggest films are oxygen deficient resulting in oxygen vacancies being present which deteriorates the dielectric properties of the alumina layers deposited.<sup>[28,53]</sup> Fröhlich et al. deposited alumina at temperatures of 100 and 200 °C with a GPC ranging from 1.08 to  $1.39 \text{ \AA cycle}^{-1}$  and O: Al for the thermal reactions at 1.42 and 1.37 for 100 and 200 °C, respectively.<sup>[22]</sup> Yoon et al. presented ultraviolet (UV) enhanced atomic layer deposition (UV-ALD) which was used to deposit alumina at temperatures as low as 40 °C. Comparing the stoichiometry of the UV-ALD to the thermal ALD process shows that the thermal process produces slightly higher stoichiometry at 1.6 as compared to 1.56 for the UV-ALD and suggested that UV irradiation which was applied during the ALD process, promoted the reaction and alumina close to the

ideal stoichiometry of 1.5 was achieved.<sup>[54]</sup> This highlights the effect of different types of deposition and stoichiometry achieved at a range of temperatures. The comparison whilst of course not representative of all literature qualifies the results that we have achieved using low temperatures and MVD. These low-temperature deposited films have further been utilized in other reports in the fabrication of biosensor devices.<sup>[55,56]</sup>

## 4. Conclusion

In summary, thin alumina films were deposited using MVD in a thermal ALD-type reaction at deposition temperatures ranging from 35 to 150 °C. GPC ranged from 0.93 to  $1.02 \text{ \AA cycle}^{-1}$  and the process window was explored and optimized in terms of precursor dosing. There was no indication of CVD-type growth which was confirmed by ellipsometry GPC, RI, and XPS measurements. Alumina films grown at 100 °C contained very low carbon impurities indicative of high conversion of TMA were highly uniform over an 8" substrate and had a near-optimal dielectric constant and refractive index. The films deposited higher than 100 °C were slightly oxygen deficient. Alumina films prepared by MVD at 100 °C show promise for various applications such as high- $\kappa$  dielectrics, passivation, or encapsulation layers. O: Al ratio results of 1.54 for the alumina deposited at temperatures as low as 60 °C is a contestant for depositing on substrates with very low thermal budgets. This process is also relevant for the deposition of conformal films in narrow pores or via structures.

## 5. Experimental Section

*Deposition of Alumina Thin Films:* Alumina thin films were deposited on 8" silicon <001> substrates (Si-Mat) with no additional treatments. Films were deposited using an MVD 300 system (SPTS) in ALD-type processes. Unless otherwise stated, the top slot of the 25-slot wafer carrier was used.

The number of purge cycles between each half-reaction (after the TMA dose and after the water dose) was adjusted according to the deposition temperature. Purge cycles used 99.999% pure N<sub>2</sub> gas. Minimum film thicknesses of 50 nm across all process conditions were obtained by calibrating the number of cycles from calibration runs. The VDM dose pressures for TMA and water vapor was set to 1.3 and 1 Torr, respectively, as determined by the dose optimization study. Precursor delivery line temperatures were kept constant at 100 °C.

*Ellipsometry:* Variable angle spectroscopic ellipsometry measurements were acquired using a J. A Woolham M-2000 system fitted with a 200 mm sample stage allowed the thicknesses of the deposited films to be accurately determined. Measurements were made by creating a 29-point map to record the film thickness and assess the nonuniformity over a 4 in. area (due to stage limitations). Four different points were manually measured at the far edges of the 8" wafer (top, bottom, left, and right) to assess the nonuniformity over the complete 8" wafer area. Each point was measured at 65°–75° angles, in steps of 5°. Film thicknesses and RI were extracted from a Cauchy model of the thin film and fitted to the data using CompleteEASE software.

*Film Stoichiometry:* Chemical analysis of the deposited alumina films was performed using a Kratos Axis Supra XPS system with an Al K $\alpha$  monochromatic source, with an emission current of 15 mA. The survey spectra were acquired with a pass energy of 160 eV. Narrow regions were collected with a pass energy of 40 eV in FOV2 (Field of View) lens mode. Charge compensation was achieved with the XPS system flood gun. Analysis of the films was performed after 100 s of Ar+ etch gun with the 5 keV energy.

Each sample had been scanned a minimum of three times, with the average value used for the measurement. This ensured an accurate

representation of the alumina thin film composition. The data analysis of the XPS measurements was performed using CasaXPS software (version 2.3.24rev1.1Z). Data were extracted using wide scan spectra, and U3 Tougaard was used as a background for the XPS data. An effective attenuation length was applied as an escape depth setting and the transition function was set to 1.

**Dielectric Measurements:** The electrical properties of the deposited films were investigated using a mercury probe to form nondestructive, repeatable contacts with the films. C–V measurements were conducted in the lateral dot-ring configuration (Figure S2c, Supporting Information), with the Hg ring contact being approximately 50 times larger than the center dot (diameter 495  $\mu\text{m}$ ). A similar configuration was used for the measurement of films on ITO. The correction for the series capacitance of the ring contact was included in the calibration. Measurements were obtained by sweeping the DC voltage from depletion to accumulation (positive to negative voltage) before returning to depletion. Three locations were tested for each deposition temperature, with repeat sweeps conducted at each location to investigate the effects of initial bias stress. All measurements were conducted at an AC frequency of 1 MHz.

## Supporting Information

Supporting Information is available from the Wiley Online Library or from the author.

## Acknowledgements

G.B. and K.R. contributed equally to this work. This work was supported by the Avenues of Commercialisation for Nano & Micro Technologies (ACNM) through the Welsh European Funding Office. This work was further supported by the Welsh Government's Sêr Cymru II Rising Star and Capacity Builder Accelerator Programs through the European Regional Development Fund, Welsh European Funding Office, and Swansea University Strategic Initiative in Sustainable Advanced Materials. A.A. is a Sêr Cymru II Rising Star Fellow and P.M. is a Sêr Cymru II National Research Chair. The authors acknowledge contributions from Pegasus Chemicals UK in this work.

## Conflict of Interest

The authors declare no conflict of interest.

## Data Availability Statement

The data that support the findings of this study are available from the corresponding author upon reasonable request.

## Keywords

alumina, atomic layer deposition, flexible, molecular vapor deposition

Received: December 28, 2022

Revised: March 12, 2023

Published online:

[1] D. A. Neamen, *Mater. Today* **2006**, *9*, 57.

[2] H. Amano, Y. Baines, E. Beam, M. Borga, T. Bouchet, P. R. Chalker, M. Charles, K. J. Chen, N. Chowdhury, R. Chu, C. de Santi, M. M. de Souza, S. Decoutere, L. di Cioccio, B. Eckardt, T. Egawa, P. Fay, J. J. Freedman, L. Guido, O. Häberlen, G. Haynes, T. Heckel, D. Hemakumara, P. Houston, J. Hu, M. Hua, Q. Huang,

A. Huang, S. Jiang, H. Kawai, et al., *J. Phys. D Appl. Phys.* **2018**, *51*, 163001.

[3] J. Jiang, Y. Cheng, X. Sun, K. Huang, K. Wang, S. Cheng, H. Yuan, R. Liu, W. Li, H. Zhang, J. Li, C. Tu, Y. Qi, Z. Liu, *ACS Appl. Mater. Interfaces* **2022**, *14*, 19889.

[4] M. Swaminathan, M. Kathaperumal, K. Sik Moon, H. Sharma, P. Murali, S. Ravichandran, *MRS Bull.* **2021**, *46*, 967.

[5] Y. Zhang, Z. Qiu, X. Cheng, H. Xie, H. Wang, X. Xie, Y. Yu, R. Liu, *J. Phys. D Appl. Phys.* **2014**, *47*, 055106.

[6] C. H. Wang, G. Doornbos, G. Astromskas, G. Vellianitis, R. Oxland, M. C. Holland, M. L. Huang, C. H. Lin, C. H. Hsieh, Y. S. Chang, T. L. Lee, Y. Y. Chen, P. Ramvall, E. Lind, W. C. Hsu, L. E. Wernersson, R. Droopad, M. Passlack, C. H. Diaz, *AIP Adv.* **2014**, *4*, 047108.

[7] J. Frascaroli, G. Seguini, E. Cianci, D. Saynova, J. van Roosmalen, M. Perego, *Phys. Status Solidi A* **2013**, *210*, 732.

[8] M. Wanebo, B. Kobrin, F. Helmrich, J. Chinn, in *Proc. of the Int. Symp. and Exhibition on Advanced Packaging Materials Processes, Properties and Interfaces*, Vol. 2005, IEEE **2005**, p. 136, <https://doi.org/10.1109/ISAPM.2005.1432063>.

[9] F. T. Tsai, C. K. Chao, K. J. Jhong, R. C. Chang, *Adv. Mech. Eng.* **2017**, *9*, 1.

[10] S. D. Elliott, J. C. Greer, *J. Mater. Chem.* **2004**, *14*, 3246.

[11] Y. Widjaja, C. B. Musgrave, *Appl. Phys. Lett.* **2002**, *80*, 3304.

[12] C. D. Travis, R. A. Adomaitis, *Chem. Vap. Deposit.* **2013**, *19*, 4.

[13] C. Barbos, D. Blanc-Pelissier, A. Fave, E. Blanquet, A. Crisci, E. Fourmond, D. Albertini, A. Sabac, K. Ayadi, P. Girard, M. Lemiti, *Energy Proc.* **2015**, 558.

[14] V. E. Stempel, K. Knemeyer, R. N. D'Alnoncourt, M. Driess, F. Rosowski, *Nanomater* **2018**, *8*, 365.

[15] A. J. Ben-Sasson, G. Ankonina, M. Greenman, M. T. Grimes, N. Tessler, *ACS Appl. Mater. Interfaces* **2013**, *5*, 2462.

[16] B. Yang, C. Yao, Y. Yu, Z. Li, X. Wang, *Sci. Rep.* **2017**, *7*, 1.

[17] G. Chen, Y. Weng, F. Sun, X. Zhou, C. Wu, Q. Yan, T. Guo, Y. Zhang, *RSC Adv.* **2019**, *9*, 20884.

[18] M. D. Groner, F. H. Fabreguette, J. W. Elam, S. M. George, *Chem. Mater.* **2004**, *16*, 639.

[19] J. Dendooven, C. Detavernier, in *Atomic Layer Deposition in Energy Conversion Applications*, Wiley **2017**, p. 1, <https://doi.org/10.1002/9783527694822.ch1>.

[20] R. W. Johnson, A. Hultqvist, S. F. Bent, *Mater. Today* **2014**, *17*, 236.

[21] R. L. Puurunen, *J. Appl. Phys.* **2005**, *97*, 121301.

[22] K. Frohlich, M. Micusik, E. Dobrocka, P. Siffalovic, F. Gucmann, J. Fedor, in *ASDAM 2012 – Conf. Proc.: The 9th Int. Conf. on Advanced Semiconductor Devices and Microsystems*, IEEE **2012**, p. 171, <https://doi.org/10.1109/ASDAM.2012.6418575>.

[23] H. Fujiwara, R. W. Collins, in *Springer Series In Optical Sciences*, Springer, p. 214, <https://www.springer.com/series/624>.

[24] H. K. Sahoo, L. Ottaviano, Y. Zheng, O. Hansen, K. Yvind, *J. Vac. Sci. Technol. B* **2017**, *36*, 011202.

[25] V. Vandalon, W. M. M. Erwin Kessels, *Langmuir* **2019**, *35*, 10374.

[26] S. K. Kim, S. W. Lee, C. S. Hwang, Y.-S. Min, J. Y. Won, J. Jeong, *J. Electrochem. Soc.* **2006**, *153*, F69.

[27] D. K. Schroder, in *Semiconductor Material and Device Characterization*, 3rd ed., Wiley **2005**, p. 1.

[28] J. M. Rafí, M. Zabala, O. Beldarrain, F. Campabadal, *J. Electrochem. Soc.* **2011**, *158*, G108.

[29] G. Dingemans, W. M. M. Kessels, *J. Vac. Sci. Technol. A* **2012**, *30*, 040802.

[30] M. N. Getz, M. Povoli, E. Monakhov, *IEEE J. Photovolt.* **2022**, *12*, 929.

[31] D. M. Fleetwood, *IEEE Trans. Nucl. Sci.* **1992**, *39*, 269.

[32] M. B. González, J. M. Rafí, O. Beldarrain, M. Zabala, F. Campabadal, *J. Vac. Sci. Technol. B* **2012**, *31*, 01A101.

- [33] F. Werner, B. Veith, D. Zielke, L. Kühnemund, C. Tegenkamp, M. Seibt, R. Brendel, J. Schmidt, *J. Appl. Phys.* **2011**, *109*, 113701.
- [34] G. Dingemans, N. M. Terlinden, M. A. Verheijen, M. C. M. van de Sanden, W. M. M. Kessels, *J. Appl. Phys.* **2011**, *110*, 093715.
- [35] D. Wei, T. Hossain, N. Nepal, N. Y. Garces, J. K. Hite, H. M. Meyer, C. R. Eddy, J. H. Edgar, *Phys. Status Solidi C* **2014**, *11*, 898.
- [36] N. Nepal, N. Y. Garces, D. J. Meyer, J. K. Hite, M. A. Mastro, C. R. Eddy, *Appl. Phys. Express* **2011**, *4*, 055802.
- [37] M. D. Groner, J. W. Elam, F. H. Fabreguette, S. M. George, *Thin Solid Films* **2002**, *413*, 186.
- [38] D. J. Acheson, *Elementary Fluid Dynamics*, Clarendon Press, **1990**, 397, ISBN: 9780198596790.
- [39] M. Ylilammi, *J. Electrochem. Soc.* **1995**, *142*, 2474.
- [40] V. Cremers, R. L. Puurunen, J. Dendooven, *Appl. Phys. Rev.* **2019**, *6*, 021302.
- [41] A. S. Asundi, J. A. Raiford, S. F. Bent, *ACS Energy Lett.* **2019**, *4*, 908.
- [42] M. Leskelä, M. Mattinen, M. Ritala, *J. Vac. Sci. Technol. B* **2019**, *37*, 030801.
- [43] J. R. van Ommen, A. Goulas, *Mater. Today Chem.* **2019**, *14*, 100183.
- [44] X. Yang, A. B. F. Martinson, J. W. Elam, L. Shao, S. B. Darling, *Matter* **2021**, *4*, 3515.
- [45] B. C. Mallick, C.-T. Hsieh, K.-M. Yin, Y. A. Gandomi, K.-T. Huang, *ECS J. Solid State Sci. Technol.* **2019**, *8*, N55.
- [46] Y. Li, Y. Xiong, H. Yang, K. Cao, R. Chen, *J. Mater. Res.* **2020**, *35*, <https://doi.org/10.1557/jmr.2019.331>.
- [47] G. Burwell, N. Burrige, O. J. Sandberg, E. Bond, W. Li, P. Meredith, A. Armin, *Adv. Electron. Mater.* **2020**, *6*, 2000732.
- [48] G. S. Higashi, C. G. Fleming, *Appl. Phys. Lett.* **1989**, *55*, 1963.
- [49] V. Naumann, M. Otto, R. B. Wehrspohn, M. Werner, C. Hagendorf, *Energy Proc.* **2012**, *27*, 312.
- [50] C. Barbos, D. Blanc-Pelissier, A. Fave, C. Botella, P. Regreny, G. Grenet, E. Blanquet, A. Crisci, M. Lemiti, *Thin Solid Films* **2016**, *617*, 108.
- [51] G. P. Gakis, C. Vahlas, H. Vergnes, S. Dourdain, Y. Tison, H. Martinez, J. Bour, D. Ruch, A. G. Boudouvis, B. Caussat, E. Scheid, *Appl. Surf. Sci.* **2019**, *492*, 245.
- [52] J. L. van Hemmen, S. B. S. Heil, J. H. Klootwijk, F. Roozeboom, C. J. Hodson, M. C. M. van de Sanden, W. M. M. Kessels, *J. Electrochem. Soc.* **2007**, *154*, G165.
- [53] E. R. Zakirov, V. G. Kesler, G. Y. Sidorov, I. P. Prosvirin, A. K. Gutakovsky, V. I. Vdovin, *Semicond. Sci. Technol.* **2019**, *34*, 065007.
- [54] K. H. Yoon, H. Kim, Y. E. Koo Lee, N. K. Shrestha, M. M. Sung, *RSC Adv.* **2017**, *7*, 5601.
- [55] M. M. Ali, J. J. Mitchell, G. Burwell, K. Rejnhard, C. A. Jenkins, E. D. Ahmadi, S. Sharma, O. J. Guy, *Nanomater.* **2021**, *11*, 2121.
- [56] F. Walters, M. Munem Ali, G. Burwell, S. Rozhko, Z. Tehrani, E. Daghigh Ahmadi, J. E. Evans, H. Y. Abbasi, R. Bigham, J. John Mitchell, O. Kazakova, A. Devadoss, O. J. Guy, *Nanomaterials* **2020**, *10*, 1808.